

Ordering Dynamics of Heisenberg Spins with Torque: Crossover, Spin waves and Defects

Jaya jit Das^{1,2†} and Madan Rao^{2*}

¹*Institute of Mathematical Sciences, Taramani, Chennai 600113, India*

²*Raman Research Institute, C.V. Raman Avenue, Sadashivanagar, Bangalore 560080, India*

(November 6, 2018)

We study the effect of a torque induced by the local molecular field on the phase ordering dynamics of the Heisenberg model when the total magnetization is conserved. The torque drives the zero-temperature ordering dynamics to a new fixed point, characterized by exponents $z = 2$ and $\lambda \approx 5$. This ‘torque-driven’ fixed point is approached at times such that $g^2 t \gg 1$, where g is the strength of the torque. All physical quantities, like the domain size $L(t)$ and the equal and unequal time correlation functions obey a crossover scaling form over the entire range of g . An attempt to understand this crossover behavior from the approximate Gaussian Closure Scheme fails completely, implying that the dynamics at late times cannot be understood from the dynamics of defects alone. We provide convincing arguments that the spin configurations can be decomposed in terms of defects and spin-waves which interact with each other even at late times. In the absence of the torque term, the spin waves decay faster, but even so we find that the Gaussian closure scheme is inconsistent. In the latter case the inconsistency may be remedied by including corrections to a simple gaussian distribution. For completeness we include a discussion of the ordering dynamics at T_c , where the torque is shown to be relevant, with exponents $z = 4 - \varepsilon/2$ and $\lambda = d$ (where $\varepsilon = 6 - d$). We show to all orders in perturbation theory that $\lambda = d$ as a consequence of the conservation law.

64.60.My, 64.60.Cn, 68.35.Fx

I. INTRODUCTION

When a many-body system like a magnet or a binary fluid is quenched from its disordered high temperature phase to its ordered configuration at low temperatures, the slow annealing of “defects” (interfaces in binary fluids, vortices (hedgehogs) in XY (Heisenberg) magnets) separating competing domains, makes the dynamics very slow. The system organizes itself into a self similar spatial distribution of domains characterized by a single diverging length scale which typically grows algebraically in time $L(t) \sim t^{1/z}$. This spatial distribution of domains is reflected in the scaling behavior of the equal-time correlation function $C(r, t) \sim f(r/L(t))$. The autocorrelation function, $A(t) \sim L(t)^{-\lambda}$ is a measure of the memory of the initial configurations. The exponents z and λ and the scaling function $f(x)$ characterize the dynamical universality classes at the zero temperature fixed point (ZFP) [1].

The above phenomenology suggests that the asymptotic dynamics of the order parameter is dominated by the dynamics of its defects, and that bulk fluctuations (concentration waves in a binary fluid, spin waves in a magnet) relax fast and decouple from the dynamics of defects at late times. This picture is at the heart of recent approximate theories such as the Gaussian Closure Scheme [2,1].

But is this picture accurate? In this paper we shall study the very realistic example of the conservative dynamics of a Heisenberg magnet driven by a torque induced by the local molecular field, and show that the longer-lived spin waves couple to the defects even at late

times, driving the system to a new fixed point. The new ‘torque-driven’ fixed point characterized by $z = 2$ and $\lambda \approx 5.05$, is accessed after a crossover time $t_c \sim 1/g^2$ (where g is the strength of the torque). Crossover scaling forms describe physical quantities at late times (like the domain size $L(t, g)$ and correlation functions $C(r, t, g)$ and $A(t, g)$) for all values of g . In the absence of the torque, the spin-waves decay faster, but even so we find that the Gaussian Closure Scheme is internally inconsistent. This inconsistency may however be rectified by including leading corrections to the gaussian distribution (as suggested by Mazenko [3] for the dynamics of the conserved scalar (Ising) order parameter).

For completeness we also study the effects of including the torque in the dynamics following a quench to the critical point T_c . As reported in earlier studies [4], the torque is relevant with exponents $z = 4 - \varepsilon/2$ and $\lambda = d$ (where $\varepsilon = 6 - d$). We show to all orders in perturbation theory that $\lambda = d$ which follows as a consequence of the conservation of total magnetization [5–7].

II. HEISENBERG MAGNET AND PRECESSIONAL DYNAMICS

The order parameter $\vec{\phi}$ (whose components are ϕ_α with $\alpha = 1, 2, 3$) describing a coarse-grained spin density in a Heisenberg ferromagnet in three dimensions experiences a torque from the joint action of the external field (if present) and the local molecular field. In response the spins precess with a Larmour frequency Ω_L about the total magnetic field. Coupling to various faster degrees

of freedom like lattice vibrations or electrons, causes a dissipation in energy and an eventual relaxation towards equilibrium.

This dynamics follows from the generalized Langevin equation and the Poisson algebra [8],

$$\frac{\partial \phi_\alpha}{\partial t} = \Gamma \nabla^2 \frac{\delta F}{\delta \phi_\alpha} + \Omega_L \epsilon_{\alpha\beta\gamma} \phi_\beta \frac{\delta F}{\delta \phi_\gamma} + \eta_\alpha. \quad (1)$$

The noise $\vec{\eta}$ arising from the heat bath has mean zero and is conservative,

$$\langle \eta_\alpha(\mathbf{x}, t) \eta_\beta(\mathbf{x}', t') \rangle = 2 k_B T \Gamma \delta_{\alpha\beta} \nabla^2 \delta(\mathbf{x} - \mathbf{x}') \delta(t - t'). \quad (2)$$

The free-energy functional F is taken to be of the Landau-Ginzburg form,

$$F[\vec{\phi}] = \int d^3x \left[\frac{\sigma}{2} (\nabla \vec{\phi})^2 - \frac{r}{2} (\vec{\phi} \cdot \vec{\phi}) + \frac{u}{4} (\vec{\phi} \cdot \vec{\phi})^2 \right]. \quad (3)$$

The second term in Eq. (1) is clearly the torque $\vec{M} \times \vec{H}$, where $\vec{H} \equiv -\delta F / \delta \vec{\phi}$ is the local molecular field.

Both the inertial term (by virtue of F being rotationally invariant in spin space) and the dissipation conserve the total spin, and so the full equations of motion (1) also conserve the total spin.

Since the noise correlator is proportional to temperature, we may drop it in our discussion of zero temperature quenches. We then scale space \mathbf{x} , time t and the order parameter $\vec{\phi}$ as

$$\mathbf{x} \rightarrow \sqrt{\frac{r}{\sigma}} \mathbf{x}, \quad t \rightarrow \frac{\Gamma r^2 t}{\sigma}, \quad \vec{\phi} \rightarrow \sqrt{\frac{u}{r}} \vec{\phi}$$

to obtain the equation of motion in dimensionless form,

$$\frac{\partial \vec{\phi}}{\partial t} = \nabla^2 \left(-\nabla^2 \vec{\phi} - \vec{\phi} + (\vec{\phi} \cdot \vec{\phi}) \vec{\phi} \right) + g \left(\vec{\phi} \times \nabla^2 \vec{\phi} \right). \quad (4)$$

The dimensionless parameter $g = (\Omega_L \sigma / \Gamma)(ru)^{-1/2}$ is the ratio of the precession frequency to the relaxation rate. Setting $\Omega_L \sim 10^7$ Hz and $\Gamma \sim 10^6 - 10^{10}$ Hz, gives g in the range of $\sim 10^{-3} - 10$.

III. PHASE ORDERING DYNAMICS AT $T = 0$

Let us now prepare the system initially in the paramagnetic phase and quench to zero temperature. We study the time evolution of the spin configurations as they evolve according to Eq. (4). We calculate the equal time correlator,

$$C(\mathbf{r}, t) \equiv \langle \vec{\phi}(\mathbf{x}, t) \cdot \vec{\phi}(\mathbf{x} + \mathbf{r}, t) \rangle, \quad (5)$$

and the autocorrelator,

$$C(\mathbf{0}, t_1 = 0, t_2 = t) \equiv A(t) = \langle \vec{\phi}(\mathbf{r}, 0) \cdot \vec{\phi}(\mathbf{r}, t) \rangle, \quad (6)$$

where the angular brackets are averages over the random initial conditions and space. At late times these correlators should attain their scaling forms

$$C(\mathbf{r}, t) \sim f(r/L(t)) \quad (7)$$

and

$$A(t) \sim L(t)^{-\lambda}. \quad (8)$$

The length scale $L(t)$, which is a measure of the distance between defects, may be evaluated either from the first zero of $C(r, t)$ or from the scaling of the energy density, $\varepsilon = \frac{1}{V} \int d\mathbf{r} \langle (\nabla \vec{\phi}(\mathbf{r}, t))^2 \rangle \sim L(t)^{-2}$, and grows with time as $L(t) \sim t^{1/z}$. We compute the scaling function $f(x)$, the dynamical exponent z and the autocorrelation exponent λ by simulating the Langevin Eq. (4).

A. Langevin Simulation

The Langevin simulation is performed by discretizing Eq. (4) on a simple cubic lattice (with size N ranging from 50^3 to 60^3) and adopting an Euler scheme for the derivatives [9]. The space and time intervals have been chosen to be $\Delta x = 2.5$ and $\Delta t = 0.2$. With this choice of parameters, we have checked that the resulting coupled map does not lead to any instability. We have also checked that the results remain unchanged on slight variations of Δx and Δt . Throughout our simulation we have used periodic boundary conditions.

The correlation functions Eqs. (5), (6) are calculated for values of g ranging from 0 to 1. Measured quantities are averaged over 5–10 initial configurations. The initial configurations are taken from two ensembles, both in the disordered phase. In ensemble **A**, $\vec{\phi}(t = 0)$ is uniformly distributed within the volume of a unit sphere centered at the origin. $\vec{\phi}$ at different spatial points are uncorrelated. In ensemble **B**, $\vec{\phi}(t = 0)$ is uniformly distributed on the surface of a unit sphere centered at the origin. $\vec{\phi}$ at different spatial points are again uncorrelated. We consider these two initial conditions to check if the late time dynamics is insensitive to the choice of initial ensemble (as long as they do not introduce any long-range correlations).

We first report simulation results for ensemble **A**.

Figure 1 is a scaling plot of $C(r, t)$ versus $r/L(t)$ for various values of the parameter g , where $L(t)$ is extracted from the first zero of $C(r, t)$. Note that the scaling function for $g = 0$ is very different from those for $g > 0$; further the $g > 0$ scaling functions do not seem to depend on the value of g . This suggests that the dynamics crosses over to a new ‘torque-driven’ ZFP. This is also revealed in the values of the dynamical exponent z . In Fig. 2, a plot of $L(t)$ versus t gives the expected value of $z = 4$ when $g = 0$. For $g > 0$, we see a distinct crossover

from $z = 4$ when $t < t_c(g)$ to $z = 2$ when $t > t_c(g)$. The crossover time $t_c(g)$ decreases with increasing g . The same z exponent and crossover are obtained from the scaling behaviour of the energy density ε .

To make sure that our results are not affected by finite size, we compute 3 relevant time scales (shown in Table 1 below) — (1) $t_c(g)$, the crossover time from a $t^{1/4}$ to a $t^{1/2}$ growth, (2) $t_s(g)$, the time at which asymptotic scaling begins, (3) t_{fs} , the time at which finite size effects become prominent. It is clear from the Table that $t_c < t_s < t_{fs}$, as it should be if our data is to be free of finite size artifacts. A general rule-of-thumb is that finite size effects start becoming prominent when the domain size gets to be of order $1/3$ the system size, and we see from Table 1 that L_{max}/N is comfortably less than $1/3$.

Table 1

g	$t_c(g)$	$t_s(g)$	t_{fs}	L_{max}/N	f_{min}
0	—	900	> 7650	$1/10$ at $t = 7650$	-0.14
0.1	3150	≥ 7650	> 7650	$1/6$ at $t = 7650$	-0.08
0.3	900	1350	> 7650	$1/4$ at $t = 7650$	-0.06
0.5	450	900	4950	$1/3.7$ at $t = 4950$	-0.06

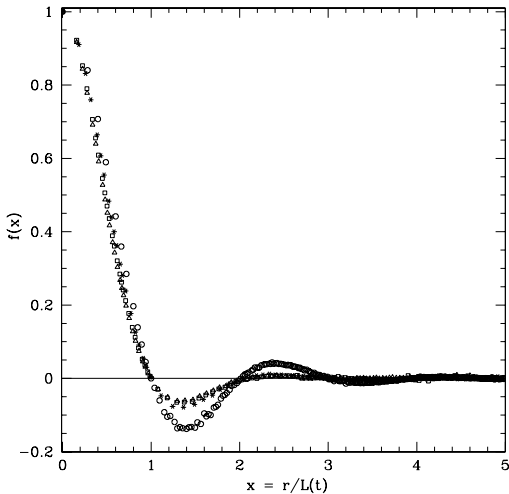


FIG. 1. Scaling plot of $C(r, t)$ for $N = 50^3$. The scaling function $f(x)$ changes as g is varied from $g = 0$ (\circ) to $g \neq 0$ ($g = 0.1(*)$, $0.3(\triangle)$, $0.5(\square)$).

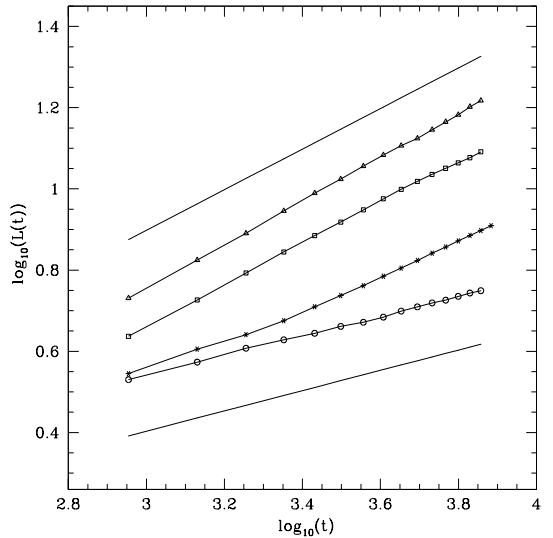


FIG. 2. Log-Log plot of $L(t)$. At $g = 0$ (\circ) we find that $z = 4$ (line of slope 0.25 drawn at the bottom for comparison). At $g \neq 0$ ($g = 0.1(*)$, $0.3(\square)$, $0.5(\triangle)$), z crosses over from 4 to 2 (line of slope 0.5 drawn at the top).

The last column in Table 1 shows f_{min} , the value of the scaling function evaluated at the first minimum as a function of g . It is easy to see why $f_{min}(g) < f_{min}(g = 0)$, since the precession of the spins about the local molecular field would cause spins from neighboring "domains" to be less anti-correlated. This is borne out by computing the spin-wave correction to an approximate form of $C(r, t; g = 0)$ (given in Eq. (29), more on this later) to quadratic order in the spin-wave amplitude [8].

The autocorrelation function $A(t)$ is calculated for $g = 0, 0.2$ and 0.3 (Fig. 3). The simulations have been done on a lattice of size 60^3 and averaged over 10 initial configurations (we have to average over a large number of initial configurations for smoother data). The λ exponent extracted from the asymptotic decay of $A(t)$ clearly suggests a crossover from $\lambda = 2.2$ to $\lambda \approx 5.05$. The numerical determination of λ is subject to large errors [10,8] and is very sensitive to finite size effects, and so we have to go to very late times and hence large system sizes to obtain accurate results.

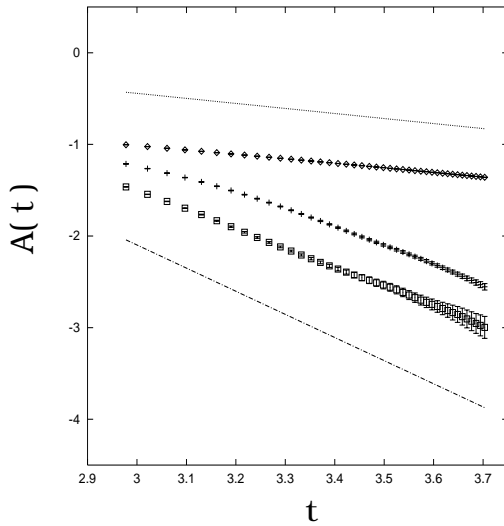


FIG. 3. Log-Log plot of $A(t)$ vs t for $g = 0(\diamond)$, $0.2(+)$, $0.3(\square)$. Solid line on top has the form $a/t^{\lambda/z}$ where $\lambda = 2.19$ and $z = 4$ (corresponding to the $g = 0$ fixed point) while the one below has a $\lambda = 5.05$ and $z = 2$ (corresponding to the ‘torque-driven’ fixed point).

To make sure that we collect asymptotic data untainted by finite size, we compute two time scales (Table 2) — (i) $t_{fit}(g)$, the time beyond which $A(t)$ can be fit with a power law $a(t + t_0)^{-\lambda/z}$, (ii) t_{fs} , the time at which finite size effects on $A(t)$ become prominent. The crossover time t_c was displayed in Table 1.

To determine t_{fs} we plot an effective exponent $\lambda_{eff} = -td(\log A(t))/dt$ as a function of $1/t$. The derivative is calculated numerically with a $\delta t = 15$ (in units of the time discretisation Δt). We see from Fig. 4, that at late times $t > t_{fs}$, λ_{eff} crosses over to being a decreasing function of time, clearly a finite size effect. This estimate of t_{fs} is not very sensitive to the choice of δt changing by 1% (for $g = 0.2$) and 3.5% (for $g = 0.3$) as δt changes by 5 units. Note that finite size effects in $A(t)$ appear earlier than in $C(r, t)$.

It is seen from Table 2 that $t_{fit} < t_{fs}$, as it should if we are to have an accurate determination of λ .

Table 2

g	$t_{fit}(g)$	t_{fs}	λ
0.0	900	> 9000	$2.199 \pm 7.5 \times 10^{-3}$
0.2	1500	5376	$5.100 \pm 6.1 \times 10^{-3}$
0.3	900	5181	$5.010 \pm 2.3 \times 10^{-3}$

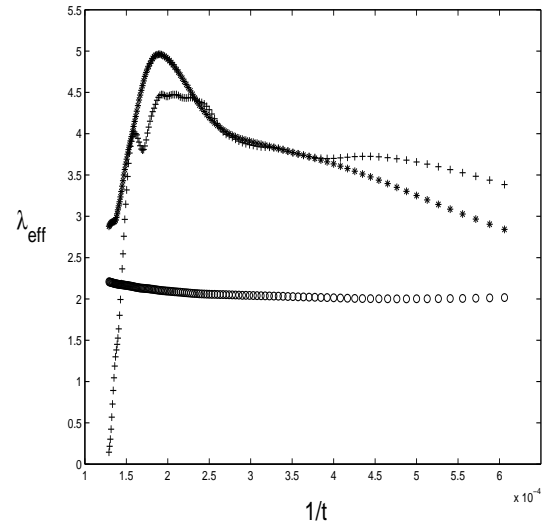


FIG. 4. λ_{eff} versus $1/t$ for $g = 0.0(\circ)$, $0.2(*)$, $0.3(+)$. Finite size effects set in when λ_{eff} starts becoming a decreasing function of time. For $g = 0$ we do not see any finite size effects in λ within our simulation times.

The last column of Table 2 lists the value of λ as a function of g . The data presented and the plot in Fig. 3 clearly support a crossover from $\lambda = 2.2$ at $g = 0$ to $\lambda = 5.05$ at $g \neq 0$. The values of λ satisfy the bound derived in [10].

We now present results of the Langevin simulation for initial conditions taken from ensemble **B**. We find that the value of z , the form of the scaling functions $f(x)$ (Fig. 5) and the decay of the autocorrelation function $A(t)$ (Fig. 6) are insensitive to the choice of initial conditions.

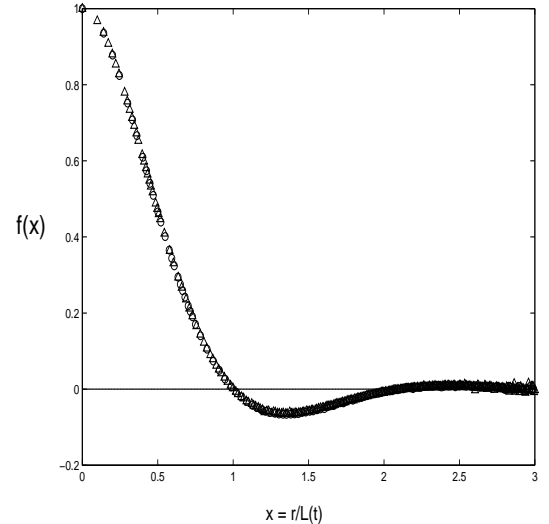


FIG. 5. Scaling function $f(x)$ vs x for $g = 0.3$ using ensembles **A**(\circ) and **B**(\triangle).

Since the initial condition **B** sets the magnitude of the spins to its $T = 0$ equilibrium value, the crossover time t_c is smaller than for ensemble **A**. For the same reason the domain sizes computed using ensemble **B** are larger than that of **A**.

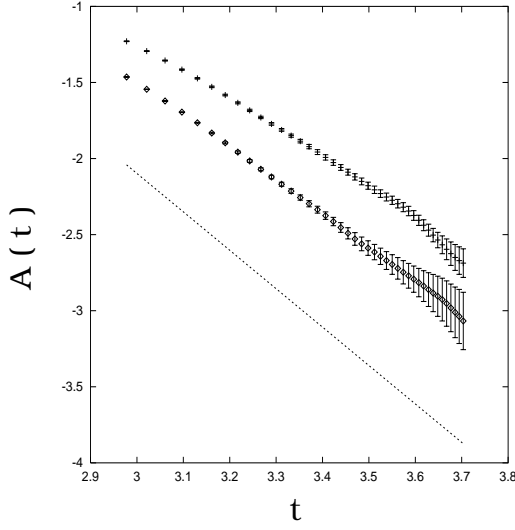


FIG. 6. Log-Log plot of $A(t)$ for $g = 0.3$ using ensembles **A**(\diamond) and **B**($+$). A power law $a/t^{\lambda/z}$ with $\lambda = 5.05$ is displayed for comparison.

B. Crossover Phenomenon

It is clear from the last section, that though the asymptotic dynamics is governed by the new ‘torque-driven’ fixed point, the dynamics at earlier times $t < t_c$ follows the $g = 0$ behavior. This suggests that the dynamics for arbitrary g , may be analyzed as a crossover from the $g = 0$ fixed point characterized by ($z = 4$, $\lambda \approx 2$) to the torque-driven fixed point where ($z = 2$, $\lambda \approx 5$).

A simple scaling argument encourages us to think of such a crossover scenario. On restoring appropriate dimensions, the dynamical equation Eq.(4) can be rewritten as a continuity equation,

$$\partial \vec{\phi}(\mathbf{r}, t)/\partial t = -\nabla \cdot \vec{j} \quad (9)$$

where the “spin current” is

$$\vec{j}_\alpha = -\Gamma \left(\nabla \frac{\delta F[\vec{\phi}]}{\delta \phi_\alpha} + \frac{\Omega}{\Gamma} \epsilon_{\alpha\beta\gamma} \phi_\beta \nabla \phi_\gamma \right). \quad (10)$$

From a dimensional analysis where we replace j_α by the ‘velocity’ dL/dt , we find

$$\frac{dL}{dt} = \Gamma \frac{\sigma}{L^3} + \Omega \frac{\sigma M_0}{L}, \quad (11)$$

where M_0 , σ and Γ^{-1} are the equilibrium magnetization, surface tension and spin mobility respectively. Beyond a crossover time given by $t_c(g) \sim (\Gamma/M_0\Omega)^2 \sim 1/g^2$, simple dimension counting shows that the dynamics crosses over from $z = 4$ to $z = 2$ in conformity with our numerical simulations.

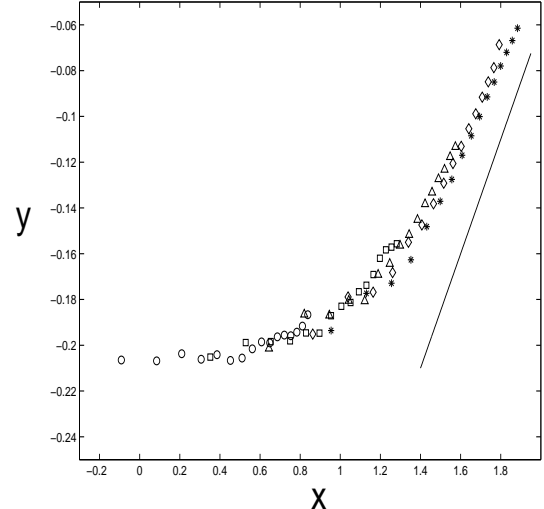


FIG. 7. Scaling plot of $y = L(t, g)/t^{1/4}$ versus $x = tg^2$ for $g = 0.03(\circ)$, $0.05(\square)$, $0.07(\triangle)$, $0.09(\diamond)$, $0.10(*)$. The solid line of slope 0.25 is the theoretical estimate of the asymptotic form of the scaling function as $x \rightarrow \infty$ (see text).

The crossover physics is best highlighted by numerically demonstrating crossover scaling of the domain size $L(t, g)$ and the correlation functions $C(r, t, g)$ and $A(t, g)$.

For instance, Eq. (11) suggests that the domain size obeys the scaling form $L(t, g) = t^{1/4} s_m(tg^2)$ where the crossover function $s_m(x)$ is determined from the transcendental equation,

$$x^{1/2} s_m(x) - \ln(1 + x^{1/2} s_m^2) - 2x = 0. \quad (12)$$

We shall now argue (and then confirm numerically) that the above scaling form holds in general. Scaling $r \rightarrow r/b$, $t \rightarrow t/b^z$ and $g \rightarrow g/b^{y_g}$, scales the domain size by

$$L(t, g) = b s(t/b^z, g/b^{y_g}) \quad (13)$$

where y_g is the scaling dimension of g . We choose b such that $t/b^z = 1$, which implies

$$L(t, g) = t^{1/z} s(g/t^{y_g/z}). \quad (14)$$

Setting $g = 0$ gives $L(t, g = 0) = t^{1/z} s(0)$, telling us that $z = 4$. Thus the scaling form Eq. (14) is governed by the $g = 0$ fixed point. We therefore need to evaluate y_g at this $g = 0$ fixed point. We determine y_g by noting the g contribution to Eq. (4)

$$\begin{aligned}
\frac{d\vec{\phi}}{dt} &\sim g\vec{\phi} \times \delta F[\vec{\phi}]/\delta\vec{\phi} \\
&= g\vec{\phi} \times \vec{\mu} \\
&\sim g/L^2
\end{aligned} \tag{15}$$

where the last relation is obtained by demanding local equilibrium (Gibbs-Thomson) on the chemical potential $\vec{\mu}$. Thus equating dimensions, $[g] = [t^{-1}][L^2] = [L^{-z+2}] = [L^{-2}]$ leading to $y_g = -2$. The crossover scaling form for the domain size can now be read out from Eq. (14),

$$L(t, g) = t^{1/4} s(g^2 t). \tag{16}$$

The $x \rightarrow \infty$ asymptote of $s(x)$ can be obtained by demanding that we recover the ‘torque-driven’ fixed point behavior, which forces $s(x \rightarrow \infty) \sim x^{1/4}$.

We will now check whether this crossover scaling form is seen in our Langevin simulation. If the above proposal is true, then the data should collapse onto the scaling curve $s(x)$ when plotted as $L(t, g)/t^{1/4}$ versus tg^2 . Figure 7 shows the results of the numerical simulation — the data collapse is not good away from the asymptotic regimes. To see a better data collapse away from either fixed point, it is necessary to include corrections to scaling.

Corrections to scaling come from two sources — (i) finite time effects and (ii) nonlinear corrections to the scaling fields [11]. Finite time corrections can be incorporated by introducing finite-time shift factors $t \rightarrow t - t_0$, which can be neglected in the $t \rightarrow \infty$ limit. Nonlinear corrections to scaling are incorporated by constructing a nonlinear, analytic function $\tilde{g}(g)$ of the physical fields g , such that it reduces to g in the limit $g \rightarrow 0$. The simplest choice of such a function is

$$\tilde{g}(g) = \frac{g + cg^2}{1 + cg^2}, \tag{17}$$

leading to a nonlinear scaling variable

$$\tilde{x} = (\tilde{g}(g))^2(t - t_0). \tag{18}$$

The data plotted with respect to this nonlinear scaling variable shows a much better collapse (Fig. 8) when c is chosen to be around -1.5 (in the Figs. 8 - 10, the finite time shift t_0 was taken to be 0). The simple mean-field estimate $s_m(\tilde{x})$ plotted for comparison (Eq. (12)), is exact only at the asymptotes.

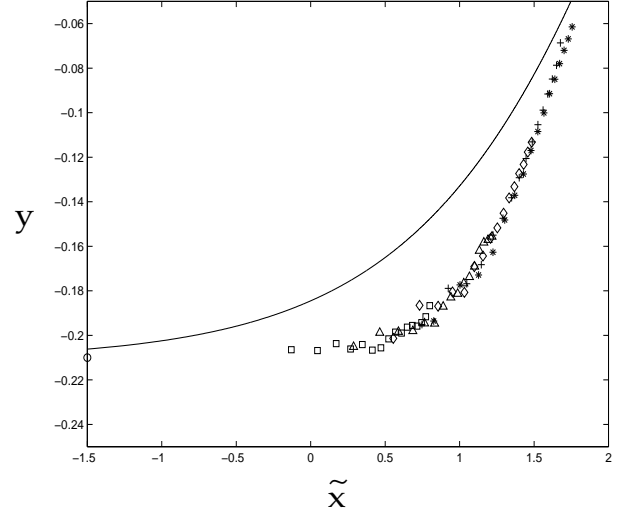


FIG. 8. Plot of $y = L(t, g)/(t - t_0)^{1/4}$ versus \tilde{x} when $c \approx -1.5$. The point \circ on the y axis, represents the value of y as $\tilde{x} \rightarrow 0$.

We have seen in the last section that the equal time correlation function $C(r, t, g)$ is unaltered when scaled with the domain size L , and so we expect it to have the following scaling behavior

$$C(r, t, g) = f(r/L, t/L^z, g/L^{y_g}), \tag{19}$$

where z is the dynamical exponent at the $g = 0$ fixed point and y_g is the scaling dimension of g . L is the size of the domain, given by Eq. (16). This readily leads to a two variable scaling form [12],

$$C(r, t, g) = f\left(\frac{r}{t^{1/4}}, tg^2\right), \tag{20}$$

with scaling variables $\rho = r/t^{1/4}$ and $x = tg^2$. When $x = 0$ and $x \rightarrow \infty$ then $f(\rho, x) = f_0(\rho)$ and $f(\rho, x) = f_T(\rho)$ respectively, where $f_0(\rho)$, $f_T(\rho)$ are the asymptotic scaling functions at $g = 0$ and $g \neq 0$. Again in terms of the nonlinear scaling variables \tilde{x} and $\tilde{\rho} = r/(t - t_0)^{1/4}$, we find a very good collapse of the data for $c \approx -1.2$ (Fig. 9).

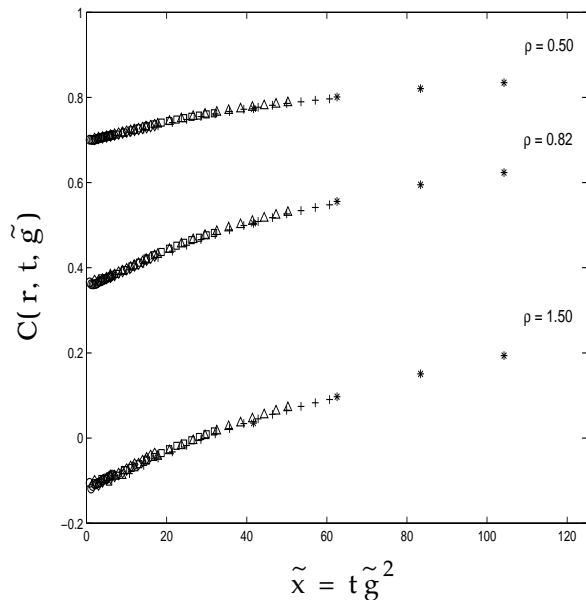


FIG. 9. $C(r, t, g)$ versus \tilde{x} at $\tilde{\rho} = 0.50, 0.82$, and 1.50 for $g = 0.03(\diamond), 0.05(\diamond), 0.07(\square), 0.09(\triangle), 0.1(+), 0.3(*)$ showing data collapse for $c \approx -1.2$.

Similar arguments suggest that the autocorrelation function satisfies the scaling form

$$A(t, g) = t^{-\lambda_0/4} a(tg^2), \quad (21)$$

where $a(x = 0) = a_0$ is a constant, and $\lambda_0 \approx 2.2$ is the value of the autocorrelation exponent at $g = 0$. As $x \rightarrow \infty$, the scaling function $a(x)$ should asymptote to $a(x) \sim x^{\lambda_0/4 - \lambda_T/2}$, where $\lambda_T \approx 5.05$ is the exponent at the ‘torque-driven’ fixed point. This expectation is borne out by the numerical simulation (Fig. 10), where we have again used the nonlinear scaling variable \tilde{x} for better collapse.

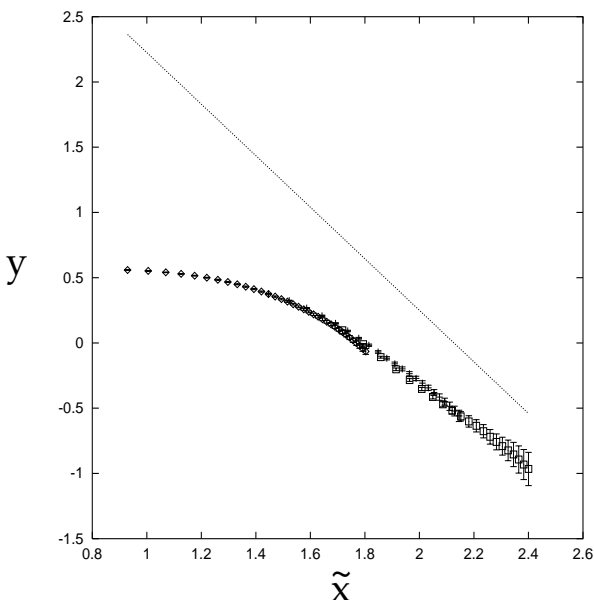


FIG. 10. Log-Log plot of $y = A(t, \tilde{g})/t^{-\lambda_0/4}$ versus \tilde{x} for $g = 0.1(\diamond), 0.2(+), 0.3(\square)$ showing data collapse for $c \approx -1.1$. The scaling function asymptotes to a line of slope $\lambda_0/4 - \lambda_T/2 = -1.95$ as $\tilde{x} \rightarrow \infty$.

The above discussion clearly indicates that for times $t \ll t_c(g) \sim 1/g^2$, the dynamics is affected by the $g = 0$ fixed point while for $t \gg t_c(g) \sim 1/g^2$, it follows the ‘torque-driven’ fixed point. Our scaling analysis suggests the following renormalization group flow diagram,

$$\tilde{x} = 0 \longrightarrow \longrightarrow \longrightarrow \longrightarrow \longrightarrow \longrightarrow \tilde{x} = \infty$$

C. Failure of Mazenko Closure Scheme: Interaction of Defects with Spin Waves

We would like to know if the crossover phenomenon described in the last section can be understood from certain approximate theories of phase ordering of conserved vector order parameters. In particular could we use such theories to calculate the crossover scaling functions and the correlation functions at the ‘torque-driven’ fixed point. The Gaussian Closure Scheme introduced by Mazenko [2] has been considered a very successful theory to compute scaling functions of conserved vector order parameters, and it is to this we turn our attention.

The method consists of trading the order parameter $\vec{\phi}(\mathbf{r}, t)$ which is singular at defect sites, for an everywhere smooth field $\vec{m}(\mathbf{r}, t)$, defined by a nonlinear transformation,

$$\vec{\phi}(\mathbf{r}, t) = \vec{\sigma}(\vec{m}(\mathbf{r}, t)). \quad (22)$$

The choice for the nonlinear function $\vec{\sigma}$ is dictated by the expectation that at late times, the magnitude of $\vec{\phi}$ saturates to its equilibrium value almost everywhere except near the defect cores. This suggests that the appropriate choice for $\vec{\sigma}$ is an equilibrium defect profile,

$$\frac{1}{2} \nabla_m^2 \vec{\sigma}(\vec{m}(\mathbf{r}, t)) = V'(\vec{\sigma}(\vec{m}(\mathbf{r}, t))), \quad (23)$$

where $V'(\vec{x}) \equiv -\vec{x} + (\vec{x} \cdot \vec{x}) \vec{x}$. The auxiliary field \vec{m} now has the natural interpretation as the position vector from the nearest defect core. Implicit in this choice is that smooth configurations such as spin waves relax fast and so decouple from defects at late times. The simplest nontrivial solution of Eq. (23) is the hedgehog configuration,

$$\vec{\sigma}(\vec{m}(\mathbf{r}, t)) = \frac{\vec{m}(\mathbf{r}, t)}{|\vec{m}(\mathbf{r}, t)|} g(|\vec{m}|), \quad (24)$$

where $g(0) = 0$ and $g(\infty) = 1$.

Equation (4) can be used to derive an equation for the correlation function $C(12) \equiv \langle \vec{\phi}(\mathbf{r}_1, t_1) \cdot \vec{\phi}(\mathbf{r}_2, t_2) \rangle$. Substituting for $\vec{\phi}$ (Eqs. (22), (24)) in the right hand side of the resulting equation, we get

$$\partial_t C(12) = -\nabla_1^2 [\nabla_1^2 C(12) - \langle \vec{\sigma}(\vec{m}(2)) \cdot V'(\vec{\sigma}(\vec{m}(1))) \rangle] + g \langle \vec{\sigma}(\vec{m}(2)) \cdot \vec{\sigma}(\vec{m}(1)) \times \nabla_1^2 \vec{\sigma}(\vec{m}(1)) \rangle. \quad (25)$$

The Gaussian Closure Scheme assumes that each component of $\vec{m}(\mathbf{r}, t)$ is an independent gaussian field with zero mean at all times. This implies that the joint probability distribution $P(12) \equiv P(\vec{m}(1), \vec{m}(2))$ is a product of separate distributions for each component and is given by [1],

$$\prod_{\alpha} \mathcal{N} \exp \left\{ -\frac{1}{2(1-\gamma^2)} \left(\frac{m_{\alpha}^2(1)}{S_0(1)} + \frac{m_{\alpha}^2(2)}{S_0(2)} - \frac{2\gamma m_{\alpha}(1)m_{\alpha}(2)}{\sqrt{S_0(1)S_0(2)}} \right) \right\}, \quad (26)$$

where

$$\mathcal{N} = \frac{1}{2\pi\sqrt{(1-\gamma^2)S_0(1)S_0(2)}} \quad (27)$$

and

$$\gamma \equiv \gamma(12) = \frac{C_0(12)}{\sqrt{S_0(1)S_0(2)}}. \quad (27)$$

The joint distribution has been written in terms of the second moments $S_0(1) = \langle m_{\alpha}(1)^2 \rangle$ and $C_0(12) = \langle m_{\alpha}(1)m_{\alpha}(2) \rangle$.

With this assumption, the right hand side of Eq. (25) simplifies to,

$$\frac{\partial C(12)}{\partial t_1} = -\nabla^2 \left[\nabla^2 C(12) + \frac{\gamma}{2S_0(1)} \frac{\partial C(12)}{\partial \gamma} \right] + g \langle \vec{\sigma}(\vec{m}(2)) \cdot \vec{\sigma}(\vec{m}(1)) \times \nabla^2 \vec{\sigma}(\vec{m}(1)) \rangle, \quad (28)$$

where the laplacian is taken with respect to \mathbf{r}_1 . With the joint probability distribution given by Eq. (26), it is clear that the last term in the above equation vanishes, implying that the torque is irrelevant at late times. This result of the Gaussian Closure Scheme, is in direct contradiction to the results of the last two sections.

What has gone wrong? There are two possible sources of error

1. The Gaussian assumption for the probability distribution of \vec{m} is invalid.

We show below that while the Gaussian assumption leads to an internal inconsistency, it may be remedied by considering corrections to the gaussian distribution. This however does not solve the above contradiction.

2. The order parameter $\vec{\phi}$ cannot be written in terms of the defect field \vec{m} alone.

We will first question the Gaussian assumption, on the lines suggested by Yeung et. al. [13] in the case of a conserved scalar (Ising) order parameter. We will do this for the case when $g = 0$, the $g \neq 0$ analysis follows similarly.

The equal time correlation function may be derived from Eqs. (28), (26) and takes the form [2]

$$C(r, t) = \frac{3\gamma}{2\pi} \left[B \left(2, \frac{1}{2} \right) \right]^2 F \left(\frac{1}{2}, \frac{1}{2}, \frac{5}{2}; \gamma^2 \right) \quad (29)$$

where $B(x, y)$ and $F(a, b, c; z)$ are the Beta and hypergeometric functions respectively and γ is given in Eq. (27). We may expand the hypergeometric function as a power series in γ [14] and then take its fourier transform,

$$S(\mathbf{k}, t) = \sum_{p=0}^{\infty} \int d\mathbf{k}_1 \dots d\mathbf{k}_{2p+1} \left[a_p \gamma_{\mathbf{k}_1}(t) \gamma_{\mathbf{k}_2}(t) \dots \gamma_{\mathbf{k}_{2p+1}}(t) \delta(\mathbf{k} + \mathbf{k}_1 + \dots + \mathbf{k}_{2p+1}) \right] \quad (30)$$

where the spectral density $\gamma_{\mathbf{k}}$ is the fourier transform of $\gamma(r, t)$ and the expansion coefficients,

$$a_p = \frac{9}{8\pi^{3/2}} \frac{[\Gamma(p+1/2)]^2}{\Gamma(p+5/2)p!} \left[B \left(2, \frac{1}{2} \right) \right]^2, \quad (31)$$

are strictly positive for $p \geq 0$. If Eq.(30) has to satisfy the conservation law $S(k = 0, t) = 0$, it is clear that $\gamma_{\mathbf{k}}(t)$ should be *negative* at some values of \mathbf{k} . This is inconsistent with the definition Eq. (27) which implies $\gamma_{\mathbf{k}}(t) \geq 0$ for all \mathbf{k} . This definition is a consequence of the Gaussian approximation.

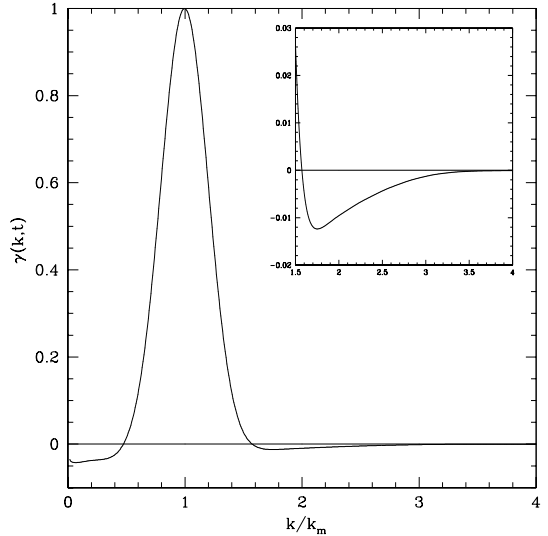


FIG. 11. The spectral density $\gamma(k, t)$ at $t = 3600$ becomes negative for $0 \leq k/k_m < 0.5$ and for $1.5 < k/k_m < 3.0$ (inset).

To determine the range of values of \mathbf{k} for which $\gamma_{\mathbf{k}}$ is negative, we numerically evaluate the fourier transform of $\gamma(r, t)$ after inverting Eq. (29). This is prone to

numerical errors because of statistical errors in our computed $C(r, t)$. For instance, a numerical integration of $\int d\mathbf{r} C(r, t)$ gives a nonzero value whereas it should be identically zero because of the conservation law. This is reflected in large errors in $\gamma(\mathbf{k}, t)$ at small \mathbf{k} . We therefore adopt the following procedure. We fit a function $C_f(x)$ to the equal time correlation function $C(r, t)$ and use this to extract $\gamma(\mathbf{k}, t)$ from the Eq. (29). The fitting function has been taken to be

$$C_f(x) = \frac{\sin(x/L)}{(x/L)} \left[1 + a \left(\frac{x}{L} \right)^2 \right] \exp[-b(x/L)^2] \quad (32)$$

which is similar to the analytic form given in Ref. [15]. Note that only b and L are independent fitting parameters, a is determined from the condition $S_f(k=0) = 0$. This function with $L = 1.5106 \pm 1.01 \times 10^{-4}$ and $b = 0.0202 \pm 2.14 \times 10^{-4}$ gives a very good fit to $C(r, t)$ upto the fourth zero of the function. We observe (Fig. 11) that the spectral density, which should be a strictly positive function of its arguments, becomes negative for $k/k_m < 0.5$ ($\gamma(k, t)$ is peaked at k_m) and in the range $1.5 < k/k_m < 3.0$.

Our demonstration suggests that a purely gaussian theory for the distribution of \vec{m} is internally inconsistent. This may however be remedied by considering corrections to the purely gaussian distribution, as suggested by Mazenko [3] for the scalar (Ising) order parameter.

In order to help us understand the nature of the corrections, let us first numerically evaluate the probability distribution of \vec{m} . We determine \vec{m} by choosing $g(|\vec{m}|)$ in such a way as to make Eq. (24) invertible. A convenient choice is

$$\vec{\phi} = \vec{\sigma}(\vec{m}) = \frac{\vec{m}}{\sqrt{1 + |\vec{m}|^2}}. \quad (33)$$

We now compute the asymptotic single point probability density $P(m_1(\mathbf{r}, t))$ on a 50^3 lattice averaged over 18 initial configurations for $g = 0, 0.3, 0.4$ and 0.5 . The probability density obeys a scaling form at late times (Figs. 12 and 13), $P(m_1, t) = P(m_1/L(t))$, where the length scale $L(t) = \sqrt{\langle m_1^2 \rangle} \sim t^{1/z}$. Moreover Fig. 14 shows that the scaled distribution of \vec{m} is identical for $g = 0$ and $g \neq 0$ (the joint probability distributions are however very different). It is clear from Figs. 12 - 14, that the asymptotic distributions show marked deviations from a simple gaussian. To highlight these deviations, we plot the scaled $\log(-\log(P(m_1)))$ versus $\log(m_1^2)$ (Fig. 15), a gaussian distribution would have given a straight line with slope -1 .

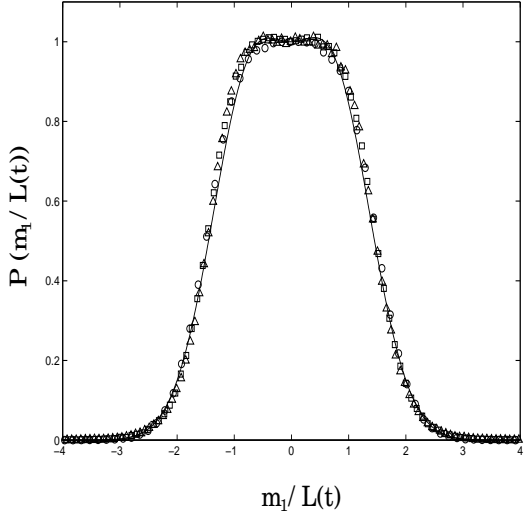


FIG. 12. Scaling plot of the un-normalized $P(x = m_1/L(t))$ for $g = 0$ at different times $t = 900(\circ)$, $3600(\square)$, $6300(\triangle)$. Solid line is a fit to Eq. (34).

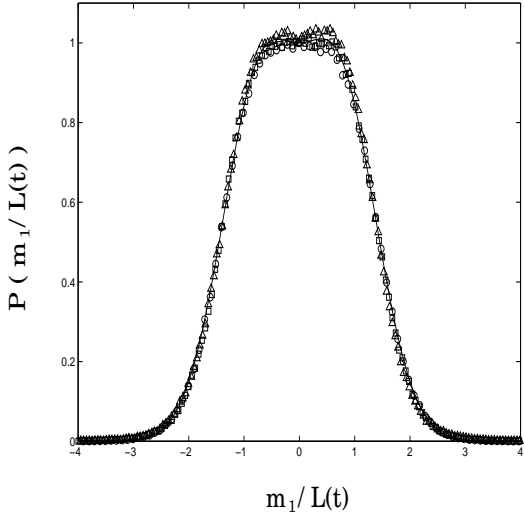


FIG. 13. Scaling plot of the un-normalized $P(x = m_1/L(t))$ for $g = 0.3$ at different times $t = 1350(\diamond)$, $3600(+)$, $5400(\square)$. Solid line is a fit to Eq. (34).

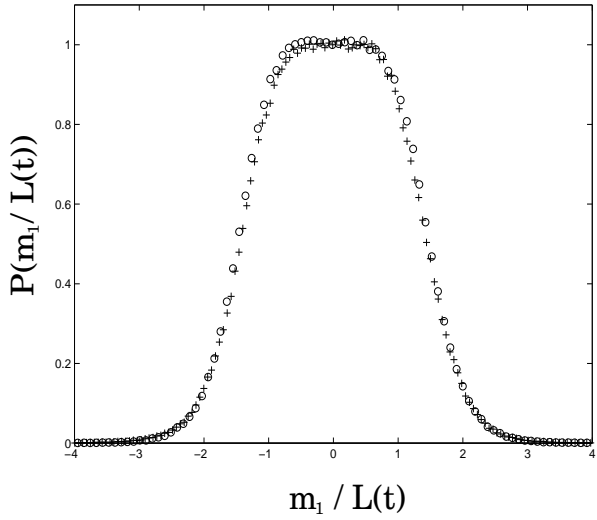


FIG. 14. Scaling plot of the un-normalized $P(x = m_1/L(t, g))$ for $g = 0$ (◊) and $g = 0.3$ (+) at $t = 4500$ showing that the distributions are identical within error bars.

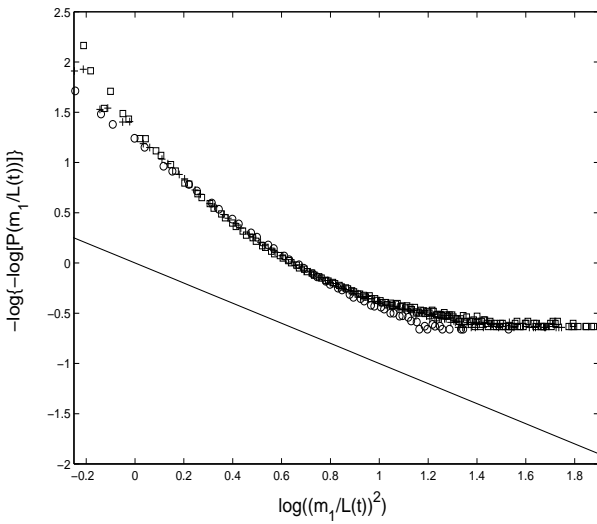


FIG. 15. Deviation of $P(x = m_1/L)$ from gaussian (straight line) for $g = 0$. Data have been collected at times $t = 900$ (◊), 3600 (+), 6300 (□).

Figures 12 - 14 suggest that the deviations from gaussian can be computed by expanding $P(m)$ in a Hermite polynomial basis H_n (a strategy advocated in Ref. [3] for the scalar (Ising) dynamics),

$$P(x) = \sum_{n=0}^{\infty} p_n H_n(x) e^{-x^2}, \quad (34)$$

where $x = m_1(r, t)/\sqrt{S_0(r, t)}$ and $H_0(x) = 1$, $H_1(x) = 2x$ and $H_{n+1}(x) = 2xH_n(x) - 2nH_{n-1}(x)$. The dark line

in Figure 12 is an accurate fit to the $g = 0$ data, with $p_0 = 1$, $p_1 = 1.33 \times 10^{-3} \pm 6.0 \times 10^{-5}$, $p_2 = 0.2352 \pm 3.8 \times 10^{-5}$, $p_3 = 1.55 \times 10^{-4} \pm 1.5 \times 10^{-5}$, $p_4 = 5.542 \times 10^{-3} \pm 7.0 \times 10^{-6}$. Similarly in Fig. 13, the dark line is an accurate fit to the $g = 0.3$ data with $p_0 = 1$, $p_1 = 3.95 \times 10^{-3} \pm 5.5 \times 10^{-5}$, $p_2 = 0.2899 \pm 1.3 \times 10^{-5}$, $p_3 = 5.35 \times 10^{-4} \pm 1.3 \times 10^{-5}$, $p_4 = 1.1913 \times 10^{-2} \pm 7.0 \times 10^{-6}$. Indeed the odd coefficients are zero to within numerical accuracy, indicating that the distribution is even.

It is conceivable that such corrections would be able to salvage the inconsistency issue, since an additive term to the right hand side of Eq. (30) would not allow us to assert that γ_k should be negative for some values of k .

Though the remedy suggested cures the inconsistency problem, it will still give a zero value to the torque contribution in Eq. (28), as long as the probability distribution of each component of \vec{m} is even and independent. We have already demonstrated that the single point distribution is even, now we shall show that each cartesian component of \vec{m} is independently distributed.

We numerically calculate $P(m_1(1), m_2(2))$ (which we label $P(x, y)$) at equal times $t_1 = t_2 = t$ and arbitrary separation, say $|\mathbf{r}_1 - \mathbf{r}_2| = 4\sqrt{3}$ for $g = 0.3$ (Fig. 16).

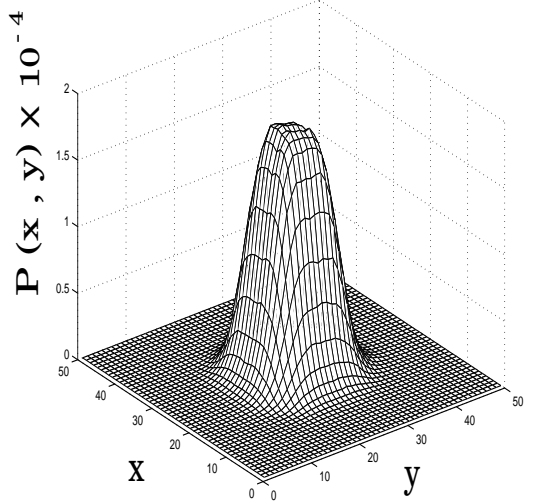


FIG. 16. Normalized joint probability distribution $P(x, y)$ where $x = m_1(1)$, $y = m_2(2)$ for $g = 0.3$ at $t = 2250$ and $|\mathbf{r}_1 - \mathbf{r}_2| = 4\sqrt{3}$ (averaged over 18 initial configurations).

To show that the joint distribution is independent in each component, we plot the difference $\Delta(x, y) = P(x, y) - P(x)P(y)$ for $g = 0.3$ (Fig. 17) and find it to be zero within the accuracy of our numerical computation.

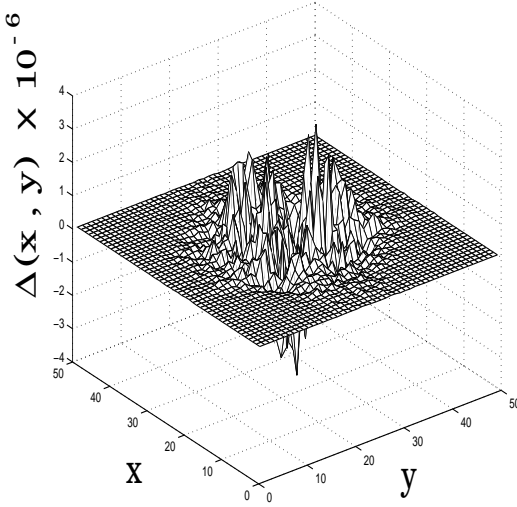


FIG. 17. Plot of $\Delta(x, y)$ where $x = m_1(1)$, $y = m_2(2)$ at $t = 2250$ and $|\mathbf{r}_1 - \mathbf{r}_2| = 4\sqrt{3}$ for $g = 0.3$. The maximum magnitude of Δ is of the order of errors in $\Delta(x, y)$.

We are thus forced to admit the second possibility, namely that the order parameter $\vec{\phi}$ cannot be written in terms of \vec{m} alone. For in transforming the spins $\vec{\phi}$ exclusively to \vec{m} we have implicitly ignored spin waves. A most direct demonstration of this is to compare $C_{3\vec{\phi}} = \langle \vec{\phi}(1) \cdot (\vec{\phi}(2) \times \nabla_2^2 \vec{\phi}(2)) \rangle$ with the defect-only contribution $C_{3\hat{m}} = \langle \hat{m}(1) \cdot (\hat{m}(2) \times \nabla_2^2 \hat{m}(2)) \rangle$ (where \vec{m} is computed by inverting Eq. (33)).

We find that for $g = 0$ both $C_{3\vec{\phi}}$ and $C_{3\hat{m}}$ are zero within error bars (Fig. 18). This is true even at very early times which implies that in the absence of the torque the spinwaves decay very fast compared to the relaxation timescale of the defects. On the other hand, when $g \neq 0$, we find that the two correlators behave very differently. Figure 19 clearly shows that even at late times, $C_{3\vec{\phi}}$ is non zero while the defect-only contribution $C_{3\hat{m}}$ is zero within errorbars.

This suggests the following decomposition in terms of defect fields (singular part) and spin-waves (smooth part), $\vec{\phi} = \vec{\sigma}(\vec{m}) + \vec{u}$, when $g \neq 0$. Such a decomposition gives rise to contributions to $C_{3\vec{\phi}}$ reflecting the interaction between defects and spin-waves.

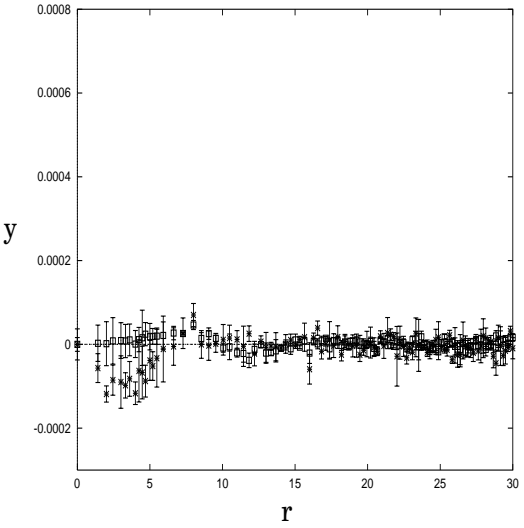


FIG. 18. $y = C_{3\vec{\phi}}(r)$ (\square) and $y = C_{3\hat{m}}(r)$ ($*$) at $t = 3600$ and $r = |\mathbf{r}_1 - \mathbf{r}_2|$ for $g = 0$ are zero within the error bars (averaged over 5 initial configurations).

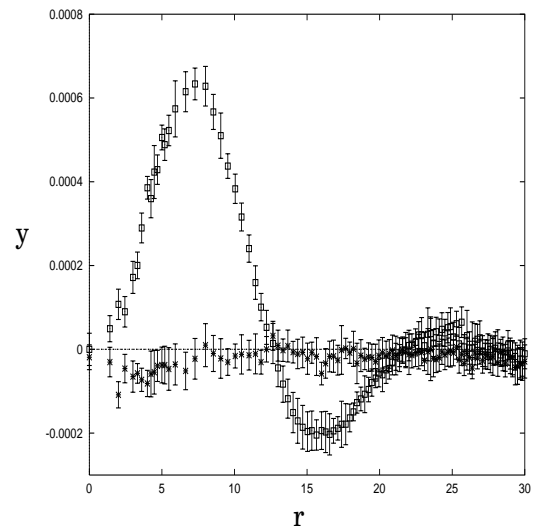


FIG. 19. $y = C_{3\vec{\phi}}(r)$ (\square) and $y = C_{3\hat{m}}(r)$ ($*$) at $t = 3600$ and $r = |\mathbf{r}_1 - \mathbf{r}_2|$ for $g = 0.3$ are distinctly different (averaged over 5 initial configurations). $C_{3\hat{m}}(r)$ (+), which has contributions from defects alone, is zero (within errorbars), whereas $C_{3\vec{\phi}}(r)$, which in addition involves spin-wave excitations, is non zero.

We conclude this long meandering section by recounting its salient results. When $g \neq 0$, typical spin configurations at late times consist of slowly moving defects and long-lived spin-waves which interact with each other. The asymptotic spin distribution cannot be written in terms of the distribution of defects alone. When $g = 0$, the spin waves decay faster, leading to a decoupling of

the spin waves and defects at late times.

IV. ORDERING DYNAMICS AT $T = T_C$

We end this study with a brief discussion of the ordering dynamics Eq. (1) of Heisenberg spins quenched to the critical point. The critical dynamics of this model (called Model J in this context) was investigated some time ago by Ma and Mazenko [4]. On the other hand, the dynamical renormalization group formalism for quench dynamics set up by Janssen *et.al.*, has been used to study Models A - C [6,7]. In this section we use the dynamical renormalization technique to study the quench dynamics of Model J (given by Eq. (1) at the critical point). Though this section does not contain anything new of a fundamental nature, it does however compute exponents to all orders in perturbation.

We first demonstrate that the precession term is relevant for the quench dynamics to T_c . We will then calculate the z and λ exponents at this new fixed point. We will show, *to all orders in perturbation*, that λ is exactly equal to the spatial dimension d . This latter fact, a consequence of the conservation law (and indeed true for Model B dynamics too), may also be arrived at by the general arguments presented in Ref. [5].

In the absence of the torque term, the nontrivial fixed point is given by the Wilson-Fisher value (WF), $u^* = (8/11)\pi^2\epsilon$, where $\epsilon = 4 - d$. Power counting shows that the scaling dimension of g is $d/2 + 1 - z + \eta/2$, where the exponents take their WF values $z = 4 - \eta$ and $\eta = (5/242)\epsilon^2$. This implies that the torque g is relevant at the WF fixed point when $d < 6$ [4].

We now have to determine this new torque driven fixed point and calculate the dynamical exponents z and λ . Both these exponents can be obtained readily using general arguments, which we briefly discuss. At the new fixed point it is clear that g does not get renormalized, which implies that $z = (d + 2 + \eta)/2$. Thus a calculation of z within perturbation theory reduces to a calculation of η at this fixed point [4]. Likewise λ can be obtained from the general arguments outlined in Ref. [5]. A crucial ingredient in this argument (valid only for quenches to T_c) is the demonstration that $S(k, t)$ obeys a scaling form at $k = 0$, a feature that was proved in Ref. [7] to all orders in perturbation for Model B dynamics. Here we *directly* calculate both z and λ using diagrammatic perturbation theory, and show that $\lambda = d$ to all orders in perturbation.

This is done within the Martin-Siggia-Rose (MSR) formalism [6]. For our problem, the MSR generating functional is,

$$\mathcal{Z}[\vec{h}, \vec{\tilde{h}}] = \int \mathcal{D}(\vec{\tilde{\phi}}) \mathcal{D}(\vec{\phi}) \exp \left\{ -J[\vec{\phi}, \vec{\tilde{\phi}}] - H_0[\vec{\phi}_0] + \int_0^\infty dt \int d\mathbf{k} (\vec{h}_\mathbf{k} \cdot \vec{\tilde{\phi}}_{-\mathbf{k}} + \vec{h}_\mathbf{k} \cdot \vec{\phi}_{-\mathbf{k}}) \right\} \quad (35)$$

with the MSR action written as

$$\begin{aligned} J[\vec{\phi}, \vec{\tilde{\phi}}] = & \int_0^\infty dt \int d\mathbf{k} \left\{ \vec{\tilde{\phi}}_\mathbf{k} \cdot \left[\partial_t \vec{\phi}_\mathbf{k} + \Gamma k^2 \frac{\delta F[\vec{\phi}]}{\delta \vec{\phi}_{-\mathbf{k}}} \right. \right. \\ & \left. \left. + \int d\mathbf{k}_1 \left(\frac{g\Gamma}{2} (k_1^2 - (\mathbf{k} - \mathbf{k}_1)^2) \vec{\phi}_{\mathbf{k}_1} \times \vec{\phi}_{\mathbf{k}-\mathbf{k}_1} \right) \right] \right. \\ & \left. - \Gamma k^2 \vec{\tilde{\phi}}_\mathbf{k} \cdot \vec{\tilde{\phi}}_{-\mathbf{k}} \right\}. \end{aligned} \quad (36)$$

In the expression for the generating functional, the initial distribution of the order parameter (gaussian with the width $= \tau_0^{-1}$) enters the form of $H_0 = \int d\mathbf{k} \frac{\tau_0}{2} (\vec{\phi}_\mathbf{k}(0) \cdot \vec{\phi}_{-\mathbf{k}}(0))$ [6].

Power counting reveals the presence of two different upper critical dimensions coming from the quartic term ($d_c^u = 4$) and the cubic torque term ($d_c^g = 6$) in the action J . This implies we have to evaluate the fixed points and exponents in a double power series expansion in $\epsilon = 4 - d$ and $\varepsilon = 6 - d$ [4].

The unperturbed correlation $C_\mathbf{k}^0(t_1, t_2)$ and response $G_\mathbf{k}^0(t_1, t_2)$ functions, and the bare u and g vertices are shown in Fig. 20. Again power counting shows that at $d = 3$, our perturbation expansion does not generate additional terms other than those already contained in J , i.e. the theory is renormalizable. However the perturbation theory gives rise to ultraviolet divergences which can be removed by adding counter-terms to the action.

To remove these divergences, we introduce renormalization factors (superscripts R and B denote renormalized and bare quantities respectively), $\vec{\tilde{\phi}}_\mathbf{k}^R(0) = (\tilde{Z}Z_0)^{-1/2} \vec{\tilde{\phi}}_\mathbf{k}^B(0)$, $\vec{\phi}_\mathbf{k}^R(t) = Z^{-1/2} \vec{\phi}_\mathbf{k}^B(t)$, $\vec{\phi}_\mathbf{k}(t) = \tilde{Z}^{-1/2} \vec{\phi}_\mathbf{k}^B(t)$, $u^R = Z_u^{-1} u^B$, $g^R = Z_g^{-1} g^B$, $\Gamma^R = Z_\Gamma^{-1} \Gamma^B$ and $\tau_0^R = Z_{\tau_0}^{-1} \tau_0^B$.

Since the dynamics obeys detailed balance, the renormalization factors Z and Z_u are the same as in statics. Further the conservation of the order parameter forces $Z\tilde{Z} = 1$ to all orders.

The new fixed point is given by the zeroes of the β functions of the theory. The β functions, calculated from the Z factors, get contributions from all diagrams containing the primitively divergent diagrams $\Gamma_{\phi\tilde{\phi}}^{(2)}$, $\Gamma_{\phi\phi\tilde{\phi}}^{(3)}$ and $\Gamma_{\phi\phi\tilde{\phi}}^{(4)}$ (Fig. 20).

The new fixed point, to one loop, is given by $g^* = \pm\sqrt{192\pi^3\varepsilon + \mathcal{O}(\varepsilon^{3/2})}$, $u^* = (8/11)\pi^2\epsilon + \mathcal{O}(\epsilon^2)$ (note u^* does not change from its WF value to all loops) and the dynamical exponent $z = 4 - \varepsilon/2 + \mathcal{O}(\varepsilon^2)$ [4].

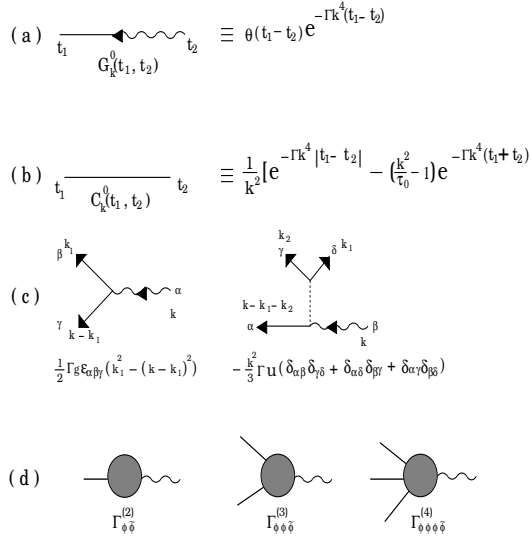


FIG.20. Unperturbed (a) response function $G_{\mathbf{k}}^0$, (b) correlation function $C_{\mathbf{k}}^0$, and the (c) two bare vertices u and g . Wavy and straight lines represent the $\vec{\phi}_{\mathbf{k}}(t)$ and $\vec{\phi}_{\mathbf{k}}(t)$ fields respectively. (d) Primitively divergent diagrams $\Gamma_{\phi\phi}^{(2)}$, $\Gamma_{\phi\phi\tilde{\phi}}^{(3)}$ and $\Gamma_{\phi\phi\tilde{\phi}\tilde{\phi}}^{(4)}$.

The λ exponent can be computed from the response function $G_{\mathbf{k}}(t, 0) \equiv \langle \vec{\phi}_{\mathbf{k}}(0) \cdot \vec{\phi}_{-\mathbf{k}}(t) \rangle$ since this is equal to the autocorrelation function $\tau_0^{-1} \langle \vec{\phi}_{\mathbf{k}}(t) \cdot \vec{\phi}_{-\mathbf{k}}(0) \rangle$, as can be seen from the first term in J on integrating by parts. The response function gets renormalized by

$$G_k^R(t, 0) = Z_0^{-1/2} G_k^B(t, 0). \quad (37)$$

The divergent contributions to G_B could come from two sources. Each term in the double perturbation series could contain the primitively divergent subdiagrams $\Gamma^{(2)}$, $\Gamma^{(3)}$ or $\Gamma^{(4)}$, which we have already accounted for by replacing these by their renormalized counterparts. The other divergent contribution could arise from the primitive divergences of the 1-particle reducible vertex function $\Gamma^{(2)}(\mathbf{k}, t, 0)$, defined by $G_{\mathbf{k}}(t, 0) \equiv \int G_{\mathbf{k}}(t - t') \Gamma^{(2)}(\mathbf{k}, t', 0) dt'$. The superficial divergence of the diagrams contributing to $G_{\mathbf{k}}(t, 0)$ is $D = V_u(d - 4) + \frac{V_g}{2}(d - 6) - 2$ (where V_u (V_g) is the number of u (g) vertices respectively). This is negative for all d . For (a) when $d > 6$, the only stable fixed point is the gaussian fixed point and so $D = -2$, (b) when $4 < d \leq 6$, u is irrelevant and so $D = \frac{V_g}{2}(d - 6) - 2 < 0$ and (c) when $d \leq 4$, D is clearly negative. This implies that $G_{\mathbf{k}}^B(t, 0)$ does not get renormalized and $Z_0 = 1$. Consequently λ stays at its mean-field value of d for this conserved Heisenberg dynamics both with and without the torque.

V. CONCLUSIONS

Traditional analysis of the asymptotic ordering dynamics of vector order parameters focuses on the dynamics of defects, and ignores the bulk excitations like spin waves which most often decay faster. In this work we have looked at the very realistic model of Heisenberg spins with precessional dynamics and have shown that the longer lived spin waves couple to the defects even at late times, driving the system to a new fixed point. The new ‘torque-driven’ fixed point characterized by $z = 2$ and $\lambda \approx 5.05$, is accessed after a crossover time $t_c \sim 1/g^2$ (where g is the strength of the torque). Crossover scaling forms describe physical quantities like domain size and equal/unequal time correlation functions for all values of g . In the absence of the torque, the spin-waves decay faster and so do not contribute to the asymptotic dynamics.

We also studied the effects of the torque on the dynamics following a quench to the critical point T_c . The torque is relevant with exponents $z = 4 - \varepsilon/2$ and $\lambda = d$ (where $\varepsilon = 6 - d$). We found to all orders in perturbation theory that $\lambda = d$ which follows as a consequence of the conservation of total magnetization.

We hope we have provided strong evidence that in order to go beyond the present approximate theories of the asymptotic dynamics of conserved order parameters, we need to systematically evaluate contributions coming from the interaction of defects with spin-waves.

We thank D. Dhar for interesting discussions and Y. Hatwalne for a critical reading of the manuscript.

[†] email : jayajit@rri.ernet.in

^{*} email : madan@rri.ernet.in

On leave of absence from : Institute of Mathematical Sciences, CIT Campus, Taramani, Chennai 600 113, India.

- [1] A. J. Bray, Adv. Phys. **43**, 357 (1994).
- [2] G. F. Mazenko, Phys. Rev. B **43**, 5747 (1991); A. J. Bray and K. Humayun, J. Phys. A **25**, 2191 (1992);
- [3] G. F. Mazenko, Phys. Rev. E **49**, 3717 (1994).
- [4] S. K. Ma and G. F. Mazenko, Phys. Rev. B **11**, 4077 (1975); P. C. Hohenberg and B. I. Halperin, Rev. Mod. Phys. **49**, 436 (1977).
- [5] S. Majumdar, D. Huse and B. Lubachevsky, Phys. Rev. Lett. (1995).
- [6] H. K. Janssen, B. Schaub, and B. Schmittmann, Z. Phys. **B73**, 539 (1989) ; H. K. Janssen in *From Phase Transitions to Chaos*, eds. G. Györgyi et. al. , World Scientific, Singapore (1992).
- [7] J. G. Kissner, Phys. Rev. B **46**, 2676 (1992).
- [8] The effects of the torque on the nonconserved dynamics of the Heisenberg model was studied in J. Das and M. Rao, Phys. Rev. E **57**, 5069 (1998).
- [9] M. Seigert and M. Rao, Phys. Rev. Lett. **70**, 1956 (1993).

- [10] C. Yeung, M. Rao and R. Desai, Phys. Rev. E **53**, 1 (1996).
- [11] F. J. Wegner, Phys. Rev. B **5**, 4529 (1972); C. J. Camacho and M. E. Fisher, J. Chem. Phys. **94**, 5693 (1991).
- [12] D. Stauffer, M. Ferer and M. Wortis, Phys. Rev. Lett. **29**, 345 (1972).
- [13] C. Yeung, A. Shinozaki and Y. Oono, Phys. Rev. E **49**, 2693 (1994).
- [14] M. Abramovitz and I. A. Stegun, Handbook of Mathematical Functions, (Dover, NY, 1970).
- [15] F. R. Iniguez and A. J. Bray, Phys. Rev. E **51**, 188 (1995).